

# Voltage-controlled spin wave Doppler shift in FM/FE heterojunction

Kang Wang,<sup>1</sup> Shaojie Hu,<sup>1,\*</sup> and Tai Min<sup>1,†</sup>

<sup>1</sup>*Center for Spintronics and Quantum Systems,  
State Key Laboratory for Mechanical Behavior of Materials,  
School of Materials Science and Engineering,  
Xi'an Jiaotong University, Xi'an, Shaanxi, 710049, China*

(Dated: June 22, 2022)

## Abstract

Efficient manipulation of spin waves (SWs) is considered as one of the promising means for encoding information with low power consumption in next generation spintronic devices. The SW Doppler shift will be one important phenomenon by manipulating SWs propagation. Here, we predict an efficient way to control the SW Doppler shift by voltage control magnetic anisotropy boundary (MAB) movement in FM/FE heterojunction. From the micromagnetic simulation, we confirmed the SW Doppler shift is fitting our theoretical predictions very well in Fe/BaTiO<sub>3</sub> heterostructure. The low power consumption of SW Doppler shift also shows ultra wide-band shift properties with voltage. We believe that such SW Doppler shift could be employed as an accurate investigation of ferroelectric domain wall movement.

---

\* [shaojiehu@mail.xjtu.edu.cn](mailto:shaojiehu@mail.xjtu.edu.cn)

† [tai.min@xjtu.edu.cn](mailto:tai.min@xjtu.edu.cn)

Magnonics[1–3], an emerging field associated with quantum magnetic dynamic phenomena, mainly focus on the study and utilization of spin waves (SWs) for information processing on the nanoscale. SWs could provide a promising paradigm for encoding information beyond metal–oxide–semiconductor (CMOS) computing because of no Joule heating in propagation, wide frequency range, scaling down to atomic dimensions, various nonlinear and nonreciprocal phenomena.[4–7] SWs exhibit most of the properties inherent in waves, which can be in analogy with a sound or light wave in many aspects. Doppler effect, one classical effect in waves, describes the frequency shift caused by the relative motion between the source and the observer. Many novel SW Doppler shift phenomena have been observed most recently. Stancil, et al reported the experimental observation of an inverse Doppler shift from left-handed dipolar SWs with a moving pick-up antenna, which is the intrinsic characteristic of left-handed, or backward SWs.[8] Vlaminck and Bailleul found the current-induced SW Doppler shift that related to the adiabatic spin-transfer torque, which can be used as a probe of spin-polarized transport in various ferromagnets.[9] Yu, et al predicted the SW Doppler shift by magnon drag in magnetic insulators.[10] Nakane and Kohno studied the current-induced SW Doppler shift in antiferromagnets.[11] These fascinating phenomena spark the research interesting of the SW Doppler shift.

However, almost all the related researches on SW Doppler shift are based on the single ferromagnetic materials with the electric current control, which limits the ultra low power consumption for manipulating SWs. Actually, magnetoelectric effect is considered as an efficient way to program the propagation of SWs with low power consumption in multiferroic materials. [12–17] The most representative multiferroic system is artificial multiferroic materials with FM/FE heterojunction. Here we present the SW Doppler shift owing to the voltage control of magnetic anisotropy boundary (MAB) moving in FM/FE heterojunction. As shown in Fig. 1, the ferromagnetic layer on a ferroelectric substrate with in-plane and out-of-plane polarization domains exhibits two magnetic anisotropy regions A1 and A2, which arises from the inverse magnetostriction induced by the different strains in polarization domains.[18] The MAB separating the two anisotropy regions is pinned on the ferroelectric domain wall. A positive (negative) voltage-controlled perpendicular electric field can drive the motion of the ferroelectric domain wall along  $x$  ( $-x$ ) axis as well as the MAB.[19] The frequencies of reflected and transmitted SWs will show the red (blue) shift for the same (opposite) direction of incident SW with the movement of MAB. In this letter, we provide

an analytical model of the SW Doppler shift and verify it by simulation.

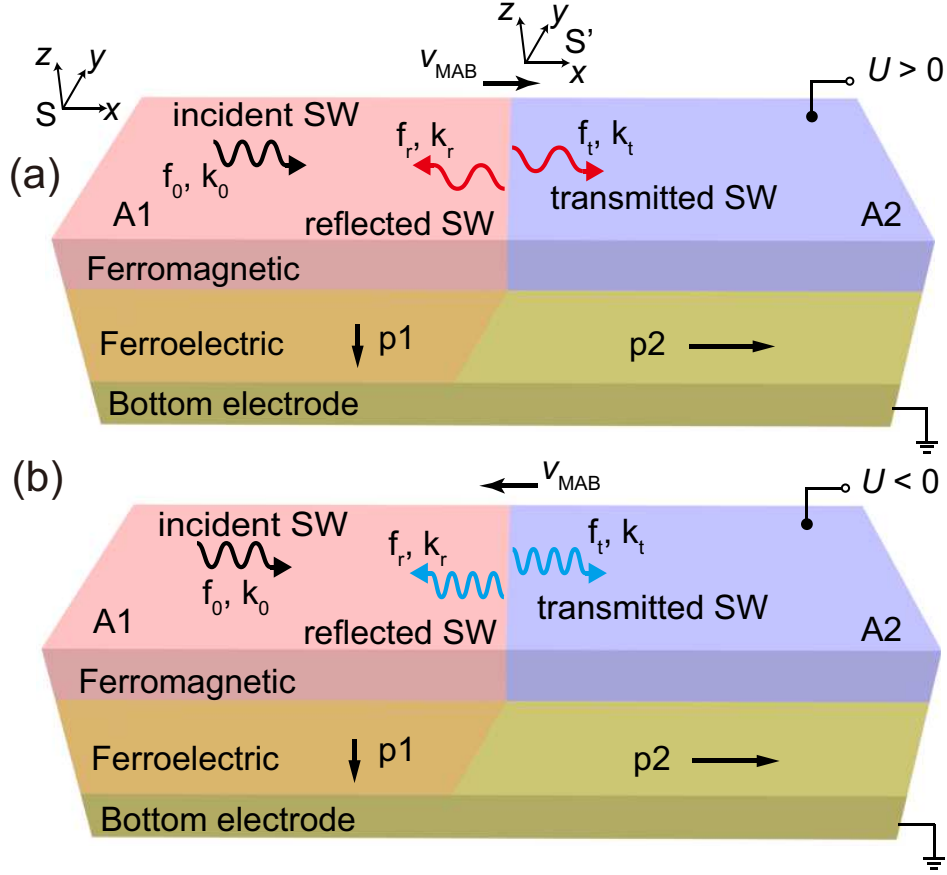


FIG. 1. The schematic of SW Doppler shift induced by the voltage-controlled MAB movement in FM/FE heterojunction. The out-of-plane and in-plane polarization domains in the ferroelectric layer transfer different strains to the ferromagnetic layer. The ferromagnetic layer exhibits different anisotropy regions owing to inverse magnetostriction. (a) The positive voltage induced SW Doppler red shift. (b) The negative voltage induced SW Doppler blue shift.

Here, we can analyse the SW Doppler shift by analogy with sound or light wave propagation. First, we defined the observer's system  $S$  which is stationary with respect to the lab frame and the moving system  $S'$ , which is stationary with respect to the MAB, shown in Fig. 1(a). In the observer's system  $S$ , the general dispersion relation of SWs in A1 and A2 are described as different functions with wave vector  $k$  ( $f_1 = F_1(k)$  and  $f_2 = F_2(k)$ ). In the moving system  $S'$ , the dispersion relations of SWs propagating in A1 and A2 are following by neglecting relativistic effect because of  $v_{MAB}$  (velocity of MAB)  $< v_p$  (phase velocity of

SWs)  $\ll c$  (velocity of light):

$$f'_1 = f_1 - \frac{\mathbf{k} \cdot \mathbf{v}_{\text{MAB}}}{2\pi} = F_1(k) - \frac{\mathbf{k} \cdot \mathbf{v}_{\text{MAB}}}{2\pi} \quad (1)$$

$$f'_2 = f_2 - \frac{\mathbf{k} \cdot \mathbf{v}_{\text{MAB}}}{2\pi} = F_2(k) - \frac{\mathbf{k} \cdot \mathbf{v}_{\text{MAB}}}{2\pi} \quad (2)$$

The frequency and wave number of incident, reflected and transmitted SWs in system S and S' are defined as:  $f_0, k_0, f_r, k_r, f_t, k_t, f'_0, k'_0, f'_r, k'_r, f'_t$  and  $k'_t$ , respectively. If the incident SW from the A1 region propagates to A2 shown in Fig. 1, the frequencies of reflected and transmitted SWs in system S can be derived as following:

$$f_r = f_0 - (\mathbf{k}_0 - \mathbf{k}'_r) \cdot \frac{\mathbf{v}_{\text{MAB}}}{2\pi} \quad (3)$$

$$f_t = f_0 - (\mathbf{k}_0 - \mathbf{k}'_t) \cdot \frac{\mathbf{v}_{\text{MAB}}}{2\pi} \quad (4)$$

where, the  $k'_r$  and  $k'_t$  can be calculated from  $f'_0 = f'_r = f'_t$ . Because of the different dispersion relations of SWs, the  $k_0$  is generally different from  $k'_t$  and  $k'_r$ . So the frequency shift of SW Doppler effect is related to the second term of Eq.(3) and Eq.(4), which not only relate to the velocity of MAB but also the dispersion relations induced by the different magnetic anisotropy.

To verify such SW Doppler shift, we conduct the micromagnetic simulation in one well-known artificial multiferroic system Fe/BaTiO<sub>3</sub>[20, 21]. As shown in Fig. 2(a) and (b), it has been demonstrated that the Fe film on ferroelectric BaTiO<sub>3</sub> substrate with in-plane and out-of-plane polarization domains exhibits uniaxial and cubic magnetic anisotropy.[18] Using the GPU-accelerated micromagnetic software Mumax3[22], we study the SW Doppler shift controlled by voltage in Fe/BaTiO<sub>3</sub> heterojunction. We study a  $6000 \times 400 \times 2 \text{ nm}^3$  Fe film discretized using  $3000 \times 200 \times 1$  finite difference cells. The periodic boundary condition is used along  $y$  axis to avoid the boundary effect. The used simulation parameters are the following[16, 19]: saturation magnetization  $M_s = 1.7 \times 10^6 \text{ A/m}$ , exchange constant  $A_{\text{ex}} = 2.1 \times 10^{-12} \text{ J/m}$ , Gilbert damping  $\alpha = 0.003$ , cubic anisotropy constant  $K_c = 4.4 \times 10^4 \text{ J/m}^3$  and uniaxial anisotropy constant  $K_u = 1.5 \times 10^4 \text{ J/m}^3$ . To avoid the reflection of SWs in both ends, the gradually increasing  $\alpha$  from 0.003 to 0.033 is set at both ends of Fe film ( $-3000 \text{ nm} < x < -2200 \text{ nm}$ ,  $2200 \text{ nm} < x < 3000 \text{ nm}$ ). An external magnetic field

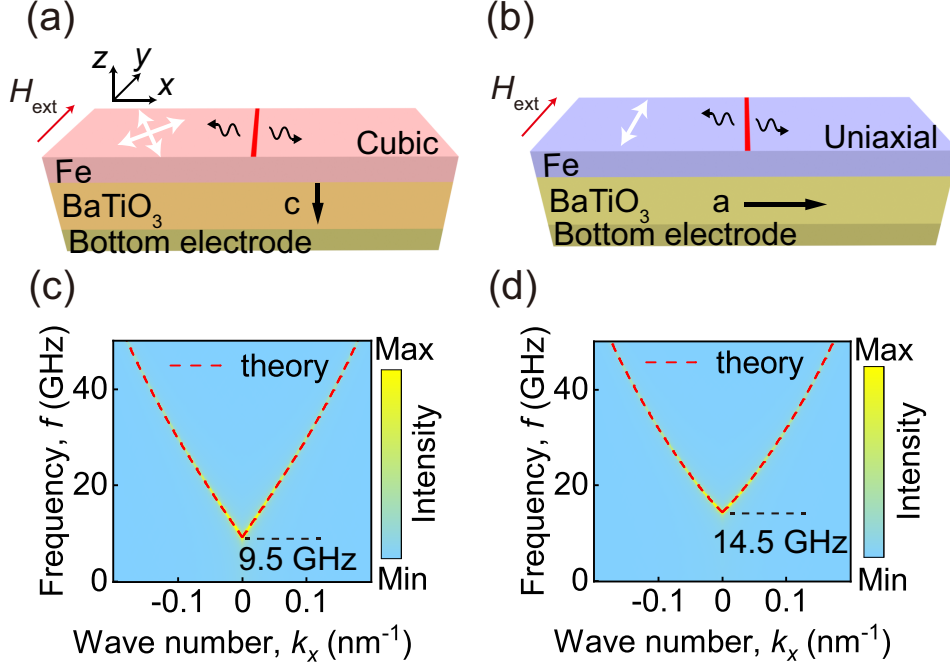


FIG. 2. (a) The cubic anisotropy is induced in Fe layer on ferroelectric BaTiO<sub>3</sub> c-domain. As shown by the white double head arrows, the easy axes of cubic anisotropy are along with directions with 45° to  $y$  axis. (b) The uniaxial anisotropy is induced in Fe layer on ferroelectric BaTiO<sub>3</sub> a-domain. As shown by the white double head arrows, the easy axis of uniaxial is along  $y$  axis. The image plot of the dispersion relations of SWs in cubic anisotropy region (c) and uniaxial anisotropy region (d) by micromagnetic simulation. The dash lines are corresponding to the theory calculation data.

$\mu_0 H_{\text{ext}} = 100$  mT is applied to magnetize the Fe film along  $y$  axis. To obtain the dispersion relation of SWs in cubic region, we set Fe film only with cubic anisotropy and perform two dimensional Fourier transform[23, 24] on  $m_x(x, t)$  in response to a sinc based exciting field  $h_0 \text{sinc}(2\pi f_c(t - t_0))\hat{e}_x$  with  $\mu_0 h_0 = 10$  mT, cutoff frequency  $f_c = 50$  GHz and  $t_0 = 5$  ns, applied in a  $6 \times 400 \times 2$  nm<sup>3</sup> center section of Fe film. The dispersion relation in cubic region is shown in Fig. 2(c). Similarly, the dispersion relation in uniaxial region can be obtained as shown in Fig. 2(d). The dash lines are the theory calculation by the equations of dispersion relation of DE SWs in uniaxial and cubic anisotropy region as following[17, 25]:

$$f = \frac{\gamma\mu_0}{2\pi} \sqrt{\left(H_{\text{ext}} + \frac{2K_u}{\mu_0 M_s} + \frac{2A_{\text{ex}}}{\mu_0 M_s} k^2\right) \left(H_{\text{ext}} + \frac{2K_u}{\mu_0 M_s} + M_s + \frac{2A_{\text{ex}}}{\mu_0 M_s} k^2\right) + M_s^2 F} \quad (5)$$

$$f = \frac{\gamma\mu_0}{2\pi} \sqrt{\left(H_{\text{ext}} - \frac{2K_c}{\mu_0 M_s} + \frac{2A_{\text{ex}}}{\mu_0 M_s} k^2\right) \left(H_{\text{ext}} + \frac{K_c}{\mu_0 M_s} + M_s + \frac{2A_{\text{ex}}}{\mu_0 M_s} k^2\right) + M_s^2 F} \quad (6)$$

where,  $\gamma$  is gyromagnetic ratio,  $\mu_0$  is vacuum permeability,  $F = \frac{1-e^{-|k|d}}{|k|d} \left(1 - \frac{1-e^{-|k|d}}{|k|d}\right)$ ,  $d$  is the thickness of the Fe film. Obviously, the difference between the anisotropy field in cubic and uniaxial regions results in the different dispersion relation.

Then we study the reflection and transmission of SWs from the moving MAB. The schematic is shown in Fig. 3(a). The width of MAB same to the pinned ferroelectric domain wall (2 – 5 nm[26–28]) is far smaller than the wavelength of SWs and we neglect it in simulation. The exciting source is a  $42 \times 400 \times 2$  nm<sup>3</sup> local section with exciting field  $h_0 \sin(2\pi f_0 t) \hat{e}_x$ ,  $\mu_0 h_0 = 10$  mT, exciting frequency  $f_0 = 18$  GHz and is 1.478  $\mu\text{m}$  away from the left end. SWs propagate in Fe film along  $x$  axis perpendicular to the MAB. The MAB moves along  $x$  axis within  $-1100$  nm to  $1900$  nm marked by the blue dash lines in Fig. 3(a). The velocity of ferroelectric domain wall in previous studies[29, 30] driven by electric field can be up to 1000 m/s promising a large velocity of MAB ( $v_{\text{MAB}}$ ), which could be calculated by the following equation[29]:

$$v_{\text{MAB}}(U) = v_{\infty} \sum_{n=1}^{\infty} n e^{-(\delta/(U/d))n^{\frac{3}{2}}} \quad (7)$$

where  $U$  is the voltage to provide perpendicular electric field in BaTiO<sub>3</sub>,  $v_{\infty} = 5$  m/s,  $\delta = 4$  kV/cm,  $d$  is the thickness of BaTiO<sub>3</sub> substrate, 100 nm.

Here, we implement MAB moving at velocity  $v_{\text{MAB}}$  by shifting the MAB over one discretization cell ( $\delta x = 2$  nm) during each time window  $\delta t = \delta x / v_{\text{MAB}}$  in simulation. The  $m_x$  in one cell at  $-1202$  nm  $< x < -1200$  nm,  $-2$  nm  $< y < -1$  nm is recorded as incident and reflected SWs, while the  $m_x$  in one cell at  $1998$  nm  $< x < 2000$  nm,  $-2$  nm  $< y < -1$  nm is recorded as transmitted SW, marked by the black and green squares A, B in Fig. 3(a), respectively. The snapshot of  $m_x$  with static MAB at  $x = 400$  nm is shown in Fig. 3(b). The blue dash line marks the position of MAB. Obviously, the SWs propagate in uniaxial and cubic regions with different wavelengths. To precisely obtain all the related frequencies of the SWs, we perform fast Fourier transform on  $m_x$  in A and B to obtain the spectra of reflected and transmitted SWs. The spectrum of the incident and reflected SWs is shown in Fig. 3(c). It should be noted that the frequency of incident SW is the exciting frequency, 18 GHz, as shown by the main peak in Fig. 3(c). When  $v_{\text{MAB}} = 0$  m/s, only one peak in the

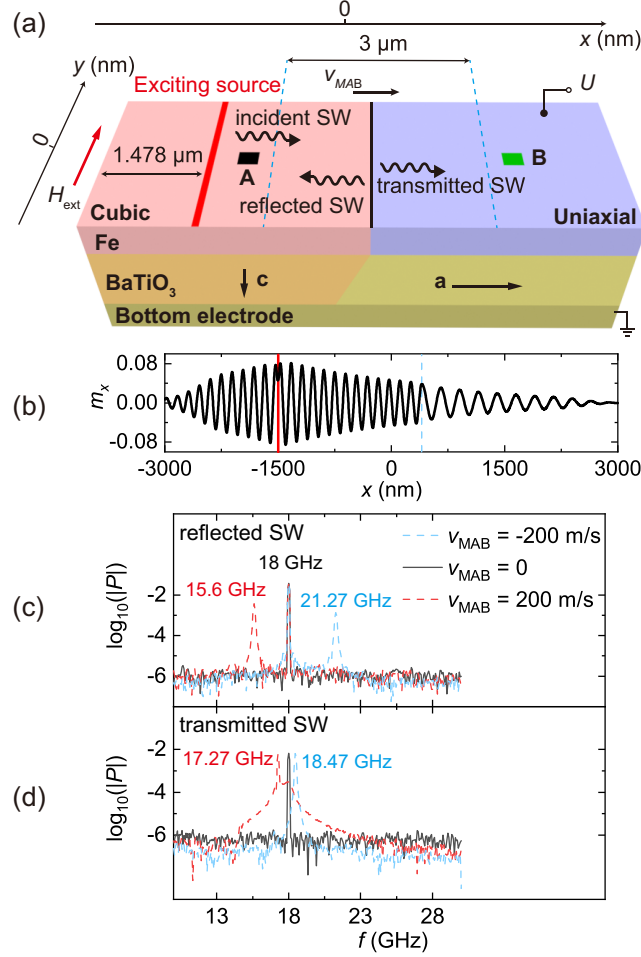


FIG. 3. (a) The schematic of reflected and transmitted SWs from the moving MAB. The MAB moves along  $x$  axis within  $-1100$  nm to  $1900$  nm marked by the blue dash lines. The black square (A) represents the cell at  $-1202$  nm  $< x < -1200$  nm,  $-2$  nm  $< y < -1$  nm, of which  $m_x$  is recorded as the incident and reflected SWs. The green square (B) represents the cell at  $1998$  nm  $< x < 2000$  nm,  $-2$  nm  $< y < -1$  nm, of which  $m_x$  is recorded as the transmitted SW. (b) The snapshot of  $m_x$  taken at  $y = -1$  nm with the static MAB at  $x = 400$  nm. The red line marks the position of exciting source and the blue dash line marks the position of static MAB. (c) The spectrum of reflected and incident SWs when  $v_{\text{MAB}} = -200, 0$  and  $200$  m/s. (d) The spectrum of transmitted SW when  $v_{\text{MAB}} = -200, 0$  and  $200$  m/s.

spectrum indicates the frequency of reflected SW is the same as the exciting frequency 18 GHz. When  $v_{\text{MAB}} = 200$  m/s, a secondary peak appears indicating the frequency of reflected SW is 15.6 GHz, which is significant red shift of SW by the Doppler effect. If we apply the

negative voltage to set the velocity of the MAB as  $v_{\text{MAB}} = -200$  m/s. The frequency of reflected SW shows a significant blue shift to 21.27 GHz. We also confirmed the spectrum of transmitted SW in Fig. 3(d). The frequency of transmitted SW shows Doppler red shift to 17.27 GHz and blue shift to 18.47 GHz at  $v_{\text{MAB}} = 200$  and  $-200$  m/s.

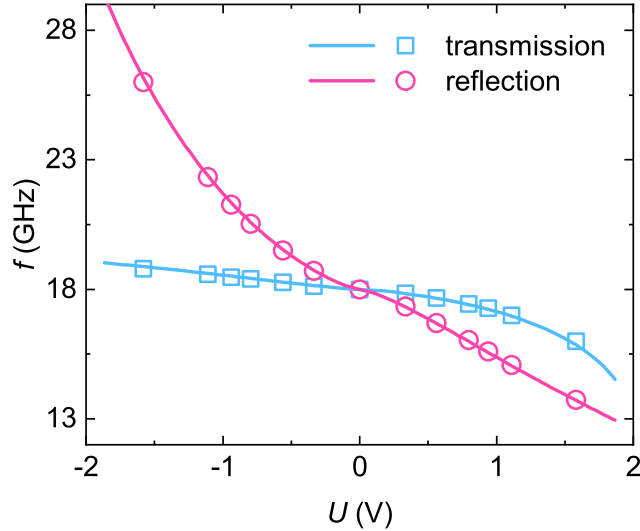


FIG. 4. The frequency of SW Doppler shift as a function of voltage for reflected and transmitted SWs in Fe/BiTiO<sub>3</sub> with the exciting frequency of 18 GHz. The symbols are corresponding to the simulated results. The solid lines are corresponding to the theoretical calculation.

To further verify our prediction, we also simulate the SW Doppler shift for the various voltage. The Fig. 4 gives the simulation results of the variation of reflected and transmitted SWs' frequencies with the voltage. The simulation results agree with the theoretical calculation. Both the reflection and transmission of SWs show a monotonic shift with the voltage. The SW Doppler shift can even be over several GHz, which is almost two order larger than the electric current controlling ways.

In summary, we predict an efficient way to control the SW Doppler shift by voltage control MAB movement in FM/FE heterojunction. The micromagnetic simulation results are well fitted by the theoretical calculation. The efficient manipulation of SW Doppler shift could be employed as an accurate investigation of the electric field-controlled ferroelectric domain wall movement.

## ACKNOWLEDGMENTS

This work is partially supported by National Key Research Program of China (Grant No. 2017YFA0206200), Natural Science Foundation of Shaanxi Province (2021JM-022).

---

- [1] V V Kruglyak, S O Demokritov, and D Grundler. Magnonics. *Journal of Physics D: Applied Physics*, 43(26):260301, 2010.
- [2] A A Serga, A V Chumak, and B Hillebrands. YIG magnonics. *Journal of Physics D: Applied Physics*, 43(26):264002, 2010.
- [3] B. Lenk, H. Ulrichs, F. Garbs, and M. Münzenberg. The building blocks of magnonics. *Physics Reports*, 507(4):107–136, 2011.
- [4] M. P. Kostylev, A. A. Serga, T. Schneider, B. Leven, and B. Hillebrands. Spin-wave logical gates. *Applied Physics Letters*, 87(15):153501, 2005.
- [5] Ki-Suk Lee and Sang-Koog Kim. Conceptual design of spin wave logic gates based on a Mach–Zehnder-type spin wave interferometer for universal logic functions. *Journal of Applied Physics*, 104(5):053909, 2008.
- [6] S. Klingler, P. Pirro, T. Brächer, B. Leven, B. Hillebrands, and A. V. Chumak. Design of a spin-wave majority gate employing mode selection. *Applied Physics Letters*, 105(15):152410, 2014.
- [7] B. Dieny, I. L. Prejbeanu, K. Garello, P. Gambardella, P. Freitas, R. Lehndorff, W. Raberg, U. Ebels, S. O. Demokritov, J. Akerman, A. Deac, P. Pirro, C. Adelman, A. Anane, A. V. Chumak, A. Hirohata, S. Mangin, Sergio O. Valenzuela, M. Cengiz Onbaşlı, M. d’Aquino, G. Prenat, G. Finocchio, L. Lopez-Diaz, R. Chantrell, O. Chubykalo-Fesenko, and P. Bortolotti. Opportunities and challenges for spintronics in the microelectronics industry. *Nature Electronics*, 3(8):446–459, 2020.
- [8] Daniel D. Stancil, Benjamin E. Henty, Ahmet G. Cepni, and J. P. Van’t Hof. Observation of an inverse Doppler shift from left-handed dipolar spin waves. *Phys. Rev. B*, 74:060404, 2006.
- [9] Vincent Vlaminck and Matthieu Bailleul. Current-Induced Spin-Wave Doppler Shift. *Science*, 322(5900):410–413, 2008.
- [10] Tao Yu, Chen Wang, Michael A. Sentef, and Gerrit E. W. Bauer. Spin-Wave Doppler Shift

- by Magnon Drag in Magnetic Insulators. *Phys. Rev. Lett.*, 126:137202, 2021.
- [11] Jotaro J. Nakane and Hiroshi Kohno. Current-Induced Spin-Wave Doppler Shift in Antiferromagnets. *Journal of the Physical Society of Japan*, 90(10):103705, 2021.
- [12] M. Balinskiy, A. C. Chavez, A. Barra, H. Chiang, G. P. Carman, and A. Khitun. Magnetolectric Spin Wave Modulator Based On Synthetic Multiferroic Structure. *Sci Rep*, 8(1):10867, 2018.
- [13] A. V. Sadovnikov, A. A. Grachev, S. E. Sheshukova, Y. P. Sharaevskii, A. A. Serdobintsev, D. M. Mitin, and S. A. Nikitov. Magnon Straintronics: Reconfigurable Spin-Wave Routing in Strain-Controlled Bilateral Magnetic Stripes. *Phys Rev Lett*, 120(25):257203, 2018.
- [14] Bivas Rana and YoshiChika Otani. Voltage-Controlled Reconfigurable Spin-Wave Nanochannels and Logic Devices. *Phys. Rev. Applied*, 9:014033, 2018.
- [15] Bivas Rana and YoshiChika Otani. Towards magnonic devices based on voltage-controlled magnetic anisotropy. *Communications Physics*, 2(1):90, 2019.
- [16] Huajun Qin, Rouven Dreyer, Georg Woltersdorf, Tomoyasu Taniyama, and Sebastiaan van Dijken. Electric-Field Control of Propagating Spin Waves by Ferroelectric Domain-Wall Motion in a Multiferroic Heterostructure. *Advanced Materials*, 33(27):2100646, 2021.
- [17] Kang Wang, Shaojie Hu, Fupeng Gao, Miaoxin Wang, and Dawei Wang. Dual function spin-wave logic gates based on electric field control magnetic anisotropy boundary. *Applied Physics Letters*, 120(14):142405, 2022.
- [18] Tuomas H. E. Lahtinen, Yasuhiro Shirahata, Lide Yao, Kévin J. A. Franke, Gorige Venkataiah, Tomoyasu Taniyama, and Sebastiaan van Dijken. Alternating domains with uniaxial and biaxial magnetic anisotropy in epitaxial Fe films on BaTiO<sub>3</sub>. *Applied Physics Letters*, 101(26):262405, 2012.
- [19] Kévin J. A. Franke, Ben Van de Wiele, Yasuhiro Shirahata, Sampo J. Hämäläinen, Tomoyasu Taniyama, and Sebastiaan van Dijken. Reversible Electric-Field-Driven Magnetic Domain-Wall Motion. *Phys. Rev. X*, 5:011010, 2015.
- [20] Chun-Gang Duan, S. S. Jaswal, and E. Y. Tsymbal. Predicted Magnetolectric Effect in Fe/BaTiO<sub>3</sub> Multilayers: Ferroelectric Control of Magnetism. *Phys. Rev. Lett.*, 97:047201, 2006.
- [21] G. Radaelli, D. Petti, E. Plekhanov, I. Fina, P. Torelli, B. R. Salles, M. Cantoni, C. Rinaldi, D. Gutiérrez, G. Panaccione, M. Varela, S. Picozzi, J. Fontcuberta, and R. Bertacco. Electric

- control of magnetism at the Fe/BaTiO<sub>3</sub> interface. *Nature Communications*, 5(1):3404, 2014.
- [22] Arne Vansteenkiste, Jonathan Leliaert, Mykola Dvornik, Mathias Helsen, Felipe Garcia-Sanchez, and Bartel Van Waeyenberge. The design and verification of MuMax3. *AIP Advances*, 4(10):107133, 2014.
- [23] Dheeraj Kumar, Oleksandr Dmytriiev, Sabareesan Ponraj, and Anjan Barman. Numerical calculation of spin wave dispersions in magnetic nanostructures. *Journal of Physics D: Applied Physics*, 45(1):015001, 2011.
- [24] G. Venkat, D. Kumar, M. Franchin, O. Dmytriiev, M. Mruczkiewicz, H. Fangohr, A. Barman, M. Krawczyk, and A. Prabhakar. Proposal for a Standard Micromagnetic Problem: Spin Wave Dispersion in a Magnonic Waveguide. *IEEE Transactions on Magnetics*, 49(1):524–529, 2013.
- [25] B. A. Kalinikos and A. N. Slavin. Theory of dipole-exchange spin wave spectrum for ferromagnetic films with mixed exchange boundary conditions. *Journal of Physics C: Solid State Physics*, 19(35):7013–7033, 1986.
- [26] X. Zhang, T. Hashimoto, and D. C. Joy. Electron holographic study of ferroelectric domain walls. *Applied Physics Letters*, 60(6):784–786, 1992.
- [27] J. Hlinka and P. Márton. Phenomenological model of a 90° domain wall in BaTiO<sub>3</sub>-type ferroelectrics. *Phys. Rev. B*, 74:104104, 2006.
- [28] Qingsong Zhang and William A. Goddard. Charge and polarization distributions at the 90° domain wall in barium titanate ferroelectric. *Applied Physics Letters*, 89(18):182903, 2006.
- [29] H. L. Stadler and P. J. Zachmanidis. Nucleation and Growth of Ferroelectric Domains in BaTiO<sub>3</sub> at Fields from 2 to 450 kV/cm. *Journal of Applied Physics*, 34(11):3255–3260, 1963.
- [30] V. Boddu, F. Endres, and P. Steinmann. Molecular dynamics study of ferroelectric domain nucleation and domain switching dynamics. *Sci Rep*, 7(1):806, 2017.